

# Quantum Network Models and Classical Localization Problems<sup>1</sup>

John Cardy<sup>a,b</sup>

<sup>a</sup>*Rudolf Peierls Centre for Theoretical Physics  
1 Keble Road, Oxford OX1 3NP, UK*

<sup>b</sup>*All Souls College, Oxford*

March 2010

## Abstract

A review is given of quantum network models in class C which, on a suitable 2d lattice, describe the spin quantum Hall plateau transition. On a general class of graphs, however, many observables of such models can be mapped to those of a classical walk in a random environment, thus relating questions of quantum and classical localization. In many cases it is possible to make rigorous statements about the latter through the relation to associated percolation problems, in both two and three dimensions.

---

<sup>1</sup>To appear in *Fifty years of Anderson Localization*, E. Abrahams, ed. (World Scientific).

# 1 Introduction

Lattice models of spatially extended systems have a long record of usefulness in condensed matter physics. Even when the microscopic physics is not necessarily related to a crystalline lattice, it can be very useful to concentrate the essential degrees of freedom onto a regular lattice whose length scale is larger than the microscopic one yet much smaller than that the expected scale of the physical phenomena the model is designed to address. In many cases, the phenomenon of universality ensures that this idealization can nevertheless reproduce certain aspects exactly. The classic example is that of a lattice gas, where a coarse-grained lattice on the scale of the particle interaction radius is introduced and used to make predictions for continuum systems, in cases in which the correlation length is large, for example close to the liquid-gas critical point.

The lattice models discussed in this article – in this context called network models – were first introduced by Chalker and Coddington[1] as a theoretical model for non-interacting electrons in two dimensions in a strong transverse magnetic field and in the presence of disorder: the physical setting for the integer quantum Hall effect. The starting point is to consider non-interacting electrons moving in two dimensions in a disordered potential  $V(r)$  and a strong perpendicular magnetic field  $B$ . We assume that the length scale of variation of  $V(r)$  is much larger than the magnetic length. In this limit the electronic motion has two components with widely separated time scales[2]: the cyclotron motion and the motion of the guiding center, along contours of  $V(r)$ . The total energy of the electron in this approximation is  $E = (n + \frac{1}{2})\hbar\omega_c + V(r)$ , where  $\omega_c = eB/m$  and  $n$  labels the Landau levels, and we therefore expect to find extended states at energies  $E_c$  corresponding to those values of  $V$  at which the contours of  $V(r)$  percolate. In 2d this is expected to occur at one particular value of  $V$ , which can be taken to be  $V = 0$ . Otherwise, away from the percolation threshold the guiding centers are confined to the neighborhoods of the closed contours, corresponding to bulk insulating phases which conduct only along the edges of the sample. This immediately provides a simple explanation of the experimental result that extended states occur only at the transition and not in the Hall plateaux. If this were literally correct the plateau transition would be in the same universality class as classical percolation.

However, this picture is modified for energies close to the transition, since quantum tunnelling is expected to be important[3] where closed contours approach each other, see Fig. 1. The network model idealizes this picture by distorting the percolating contours of  $V(r)$  into a regular square lattice, known as the L-lattice, shown in Fig. 2. In this approximation the potential  $V$  takes a checkerboard form, being  $> 0$  on (say) even squares and  $< 0$  on odd squares. In the limit of large magnetic field the spin degree of freedom of the electrons can be ignored and there is a one-dimensional vector space associated with each edge. The quantum tunnelling at each node is taken into account by an  $S$ -matrix which connects the spaces on the adjacent incoming and outgoing edges. This depends on  $E$  in such a way that for  $E > E_c$  tunnelling between edges bordering regions with  $V > 0$  is enhanced, and *vice versa* for  $E < E_c$ . Apart from this, the most important quantum feature of the problem is the phase which the electron wave function picks up

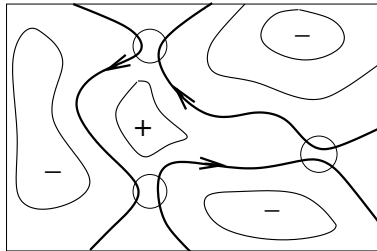


Figure 1: A typical configuration of contours of the random potential  $V(r)$ . In the guiding center approximation the particle follows these. Only those with  $V \approx 0$  (thicker lines) are important for the plateau transition. Quantum tunnelling can occur close to the saddle points of  $V(r)$  (circled). Figure adapted from Ref. [1].

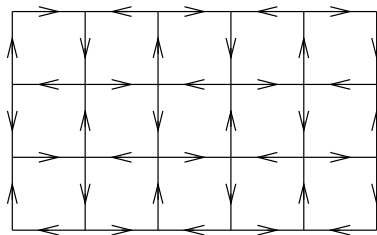


Figure 2: The idealization of Fig. 1 on the L-lattice. The edges correspond to the contours with  $V \approx 0$  and tunnelling occurs at the nodes.

on traversing a closed contour, which is proportional to the magnetic flux through the loop, and therefore its area. On idealizing the loops to a regular lattice, this is represented by a quenched uncorrelated random flux through each plaquette, or, equivalently, a quenched random  $U(1)$  phase as the particle traverses a given edge. While in principle the connectivity of the lattice, the  $S$ -matrix elements at the nodes, and the  $U(1)$  phases on the edges are all quenched random variables, in fact only the latter appear to be the most relevant in describing the universal properties of the transition.

The Chalker-Coddington model was initially analyzed numerically[1] using transfer matrix methods. Its predictions appear to agree remarkably well with experimental results, perhaps embarrassingly so since it ignores electron-electron interactions which may become important near the transition. However it has so far resisted all attempts at an analytic solution (as have other more sophisticated field theoretic formulations of the integer quantum Hall plateau transition[4]), which by now perhaps elevates this to being one of the outstanding unsolved problems of mathematical physics.

Later, following interest in various forms of exotic superconductivity, it was suggested that certain disordered spin-singlet superconductors, in which time-reversal symmetry is broken for orbital motion but Zeeman splitting is negligible, should exhibit a quantum spin Hall effect, in which the role of the electric current is replaced by that of a spin current.[5] The single-particle hamiltonians for such a system then turn out to possess an  $Sp(2)$  (or equivalently  $SU(2)$ ) symmetry. In the classification scheme of localization

universality classes due to Altland and Zirnbauer[6] they are labelled as class C. The corresponding variant of the Chalker-Coddington model is straightforward to write down, and was studied, once again numerically[7, 5]. Then, in a remarkable paper, Gruzberg, Read and Ludwig[8] argued that several important ensemble-averaged properties of this model (including the conductance) are simply related to those of critical *classical* 2d percolation. This is a powerful result because many of the universal properties of percolation are known rigorously[9]. It therefore gives exact information about a non-trivial quantum localization transition.

The arguments of Gruzberg *et al.* [8] were based on a transfer matrix formulation of the problem and therefore restricted to the particular oriented lattice (the L-lattice) used by the Chalker-Coddington model, which is appropriate to the quantum Hall problem in 2d. They also used supersymmetry to perform the quenched average. Subsequently, Beamond, Cardy and Chalker[10] gave an elementary, albeit long-winded, proof of their main result which holds for any lattice of coordination number four, and any orientation of this lattice as long each node has two incoming and two outgoing edges. Later, this was shown in a slightly more elegant fashion using supersymmetry[11]. In each case certain quenched averages of the quantum problem are related to observables of a certain kind of *classical* random walk on the same lattice. If the quantum states are localized, the corresponding classical walks close after a finite number of steps. If the quantum states are extended, in the classical problem the walks can escape to infinity.

Since this correspondence holds on a very general set of graphs and lattices, it can be used more generally to improve our understanding of quantum localization problems. In particular it can test the generally accepted notion that in two dimensions all states are localized, except in certain cases with special symmetries (such as at the Hall plateau transition). It can help understand why in higher dimensions there should be in general a transition between localized and extended states, and possibly illumine the nature of that transition. More mathematically, it may shed light on the search for a rigorous proof of the existence of extended states. Apart from the L-lattice considered by Gruzberg *et al.*, it is possible in several cases to use known information about percolation to place bounds on the behavior of the classical walks and hence the quantum network model. Up until recently, these arguments have been restricted to two dimensions, but now suitable three-dimensional lattices have been identified in which the correspondence to classical percolation is explicit.

The layout of this paper is as follows. In Sec. 2 we describe general network models and observables which are related to experimentally measurable quantities. In Sec. 3 we summarize the supersymmetric proof[11] of the main theorem which relates suitable quenched averages of these observables in the  $Sp(2)$  network model on a general graph to averages in a classical random walk problem on the same graph. The next section 4 describes how these classical models on certain lattices (the L-lattice, relevant to the quantum Hall effect, and the Manhattan lattice) relate to 2d classical percolation which can then be used to bound their behavior. In Sec. 5 we extend this to some special 3d lattices, describing relatively recent work, some of it so far unpublished. Finally in Sec. 6 we discuss some outstanding problems.

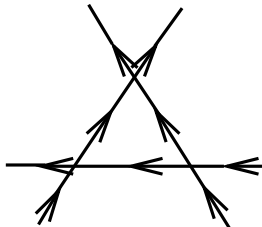


Figure 3: A  $3 \rightarrow 3$  node which can be decomposed into  $2 \rightarrow 2$  nodes.

## 2 General network models

In this section we define a general network model on a graph  $\mathcal{G}$  and discuss the kind of observables we would like to calculate. The graph  $\mathcal{G}$  consists of nodes  $n$  and oriented edges. Initially suppose that  $\mathcal{G}$  is closed, that is every edge connects two nodes, and that each node has exactly two incoming and two outgoing edges. In fact the general theorem to be proved in Sec. 3 holds for more general graphs, but it can be shown[11] that the corresponding classical problem has non-negative weights (and so admits a probabilistic interpretation) if and only if each node in  $\mathcal{G}$  and its correspond transition amplitudes can be decomposed into a skeleton graph with only  $2 \rightarrow 2$  nodes. See Fig. 3.

On each edge  $e$  of  $\mathcal{G}$  is an  $N$ -dimensional Hilbert space  $\mathcal{H}_e$ . We assume these are all isomorphic. The Hilbert space of the whole system is then  $\otimes_{e \in \mathcal{G}} \mathcal{H}_e$ . We consider a single particle whose wave function at at time  $t$  is a superposition of the basis states in this space. The dynamics is discrete: if the particle is at the center of edge  $e$  at time  $t$ , at the next time  $t + 1$  it must move in the direction of the orientated edges through a node to the center of a neighboring edge  $e'$ . Because of the discrete dynamics we should consider the unitary time-evolution operator  $\mathcal{U}$ . This has an off-diagonal block elements  $\mathcal{U}_{e'e}$  which have the form

$$\mathcal{U}_{e'e} = U_{e'}^{1/2} S_{e'e} U_e^{1/2}.$$

Here  $U_e$  is a unitary  $N \times N$  matrix which maps  $\mathcal{H}_e \rightarrow \mathcal{H}_e$  and describes the rotation of the wave function in the internal space as the particle moves along the edge  $e$ , and  $S_{e'e}$  maps  $\mathcal{H}_e \rightarrow \mathcal{H}_{e'}$  and describes the transmission through a node. The evolution matrix after time  $t$  therefore has non-zero block elements

$$\mathcal{U}_{e_f, e_i}^t = \sum_{\gamma(e_t, e_0)} \delta_{e_t, e_f} \delta_{e_0, e_i} U_{e_t}^{1/2} S_{e_t, e_{t-1}} U_{e_{t-1}} \cdots U_{e_1} S_{e_1, e_0} U_{e_0}^{1/2},$$

where the sum is over all Feynman paths  $\gamma(e_t, e_0)$  on  $\mathcal{G}$  of length  $t$ , starting at  $e_i$  and ending at  $e_f$ . Note that in this sum a given edge can be traversed an arbitrary number of times.

Both the matrices  $U_e$  and  $S_{e'e}$  are quenched random variables, assumed chosen from the invariant measure on some subgroup of  $U(N)$ . This is chosen according to the symmetry class under consideration. For spinless, or spin-polarized, electrons, where electric charge is conserved, we can take  $N = 1$  and the  $U_e \in U(1)$ . For models with class

C symmetry[6], corresponding for example to the spin quantum Hall effect, the single-particle Hilbert space is even-dimensional, and there is an action of  $\sigma_y$  such that the single-particle hamiltonian  $\mathcal{H}$  satisfies  $\mathcal{H}^* = -\sigma_y \mathcal{H} \sigma_y$ . This implies a symmetry between states with energies  $\pm E$ , and that the time-evolution operator  $\mathcal{U}^t = e^{-i\mathcal{H}t}$  satisfies

$$\mathcal{U}^* = \sigma_y \mathcal{U} \sigma_y,$$

implying that the matrices  $U_e$  should be symplectic, in  $\text{Sp}(N)$ , which for  $N = 2$  is isomorphic to  $\text{SU}(2)$ .

For a given node  $n$  with incoming edges  $(e_1, e_2)$  and outgoing edges  $(e'_1, e'_2)$ , the  $S$ -matrix has the block form

$$\begin{pmatrix} S_{e'_1 e_1} & S_{e'_2 e_1} \\ S_{e'_1 e_2} & S_{e'_2 e_2} \end{pmatrix}, \quad (1)$$

where each element is an  $N \times N$  matrix. However, since all the matrices are chosen at random, there is the gauge freedom of redefining  $S_{e'e} \rightarrow V_{e'}^{-1} S_{e'e} V_e$ ,  $U_e \rightarrow V_e^{-1} U_e V_e$ , which allows us to choose each  $S_{e'e}$  to be proportional to the unit  $N \times N$  matrix  $\mathbf{1}_N$ . The remaining  $2 \times 2$  matrix can further be chosen to be real and therefore orthogonal. Thus in fact (1) can be replaced by

$$\mathbf{1}_N \otimes \begin{pmatrix} \cos \theta_n & \sin \theta_n \\ -\sin \theta_n & \cos \theta_n \end{pmatrix}. \quad (2)$$

We are left with the gauge-transformed  $U_e$  and the  $\theta_n$  as quenched random variables. However, we shall treat them differently, first keeping the  $\theta_n$  fixed while performing quenched averages over the  $U_e$ . In fact we shall see that in most cases it suffices to take all the  $\theta_n$  as fixed and equal on each sublattice.

Because we consider discrete rather than continuous time evolution, the usual Green function is replaced by the resolvent  $(1 - z\mathcal{U})^{-1}$  of the unitary evolution operator, whose matrix elements we shall however continue to refer to as the Green function:

$$G(e_f, e_i; z) \equiv \langle e' | (1 - z\mathcal{U})^{-1} | e \rangle. \quad (3)$$

Here  $|e\rangle \in \mathcal{H}$  has non-zero components only in  $\mathcal{H}_e$ . Note that  $G(e_f, e_i; z)$  is an  $N \times N$  matrix mapping  $\mathcal{H}_{e_i} \rightarrow \mathcal{H}_{e_f}$ . The parameter  $z$  is the analog of the energy (roughly  $z \sim e^{iE}$ ). For  $|z| \ll 1$ , the expansion of (3) in powers of  $z$  gives  $G$  as a sum over Feynman paths from  $e_i$  to  $e_f$ . Each path  $\gamma$  is weighted by  $z^{|\gamma|}$  times an ordered product of the  $U_e$  with  $e \in \gamma$  and the factors of  $\cos \theta_n$  or  $\pm \sin \theta_n$  for  $n \in \gamma$ . For a finite closed graph  $\mathcal{G}$ , this expansion is convergent for  $|z| < 1$  and therefore defines  $G$  as an analytic function in this region. In general, for a finite  $\mathcal{G}$ , there are poles on the circle  $|z| = 1$  corresponding to the eigenvalues of  $\mathcal{U}$ .

However, for  $|z| > 1$ ,  $G$  admits an alternative expansion in powers of  $z^{-1}$  by writing it as

$$G(e_f, e_i; z) \equiv -\langle e' | z^{-1} \mathcal{U}^\dagger (1 - z^{-1} \mathcal{U}^\dagger)^{-1} | e \rangle. \quad (4)$$

This is given by a sum over paths  $\gamma$  with length  $\geq 1$  of a product of  $z^{-|\gamma|}$  with ordered factors  $U_e^\dagger$  along the path, and  $\cos \theta_n$  or  $\pm \sin \theta_n$  as before.

The eigenvalues of  $\mathcal{U}$  have the form  $e^{i\epsilon_j}$ , where the  $-\pi < \epsilon_j \leq \pi$  with  $j = 1, \dots, \mathcal{N}$  are discrete for a finite graph  $\mathcal{G}$ . We define the *density of states* by

$$\rho(\epsilon) \equiv \frac{1}{\mathcal{N}} \sum_j \delta(\epsilon - \epsilon_j).$$

In the standard way, the density of states is given by the discontinuity in the trace of the Green function, this time across  $|z| = 1$  rather than  $\text{Im } E = 0$ :

$$\rho(\epsilon) = \frac{1}{2\pi N |\mathcal{G}|} \sum_{e \in \mathcal{G}} \lim_{\eta \rightarrow 0^+} (\text{Tr } G(e, e; z = e^{i\epsilon - \eta}) - \text{Tr } G(e, e; z = e^{i\epsilon + \eta})) , \quad (5)$$

where the trace is in the  $N$ -dimensional space  $\mathcal{H}_e$ . In the case where  $\mathcal{G}$  is a regular lattice, in the thermodynamic limit we expect the eigenvalues to be continuously distributed around the unit circle.

We note that in the U(1) case, when the  $U_e$  are pure phases  $e^{i\phi_e}$ , in each term in the Feynman path expansion of (3,4) a given edge  $e$  occurs with a weight  $e^{in_e^\gamma \phi_e}$ , where  $n_e^\gamma$  is the number of times the path  $\gamma$  traverses this edge. On averaging a given path  $\gamma$  will contribute to the mean density of states only if  $n_e^\gamma = 0$ , that is it has length zero. Thus, in the U(1) network models,  $G(e, e, z) = 1$  for  $|z| < 1$ , and zero for  $|z| > 1$ , and the mean density of states is constant, and completely independent of the  $\theta_n$ . This is consistent with the general result that at the plateau transition in the charge quantum Hall effect, the density of states is non-singular.

We now turn to the conductance. In order to define this, we must consider an open graph, which can be obtained from a given closed graph  $\mathcal{G}$  by breaking open a subset  $\{e\}$  of the edges, relabelling each broken edge  $e$  as  $e_{\text{in}}$  and  $e_{\text{out}}$ . External contacts are subsets  $C_{\text{in}}$  and  $C_{\text{out}}$  of these. The transmission matrix  $T$  is a rectangular matrix with elements

$$T = \langle e_{\text{out}} | (1 - \mathcal{U})^{-1} | e_{\text{in}} \rangle ,$$

where  $e_{\text{in}} \in C_{\text{in}}$ ,  $e_{\text{out}} \in C_{\text{out}}$ . Note that for an open graph the resolvent  $(1 - z\mathcal{U})^{-1}$  generally has poles inside the unit circle  $|z| = 1$ . In the thermodynamic limit, however, as long as the fraction of broken edges is zero (for example if we have contacts only along part of the edge of the sample), it is believed that the limit as  $|z| \rightarrow 1$  can be taken.

The multi-channel Landauer formula then gives the conductance between the contacts as

$$g = (Q^2/h) \text{Tr } T^\dagger T ,$$

where  $Q$  is the quantum of charge carried by the particle. For the integer quantum Hall effect,  $Q = e$ , and for the spin Hall effect  $Q = \frac{1}{2}\hbar$ .

### 3 The main theorems.

In this section we focus on the Sp(2) (=SU(2)) case and summarize the method of proof of the main theorem relating the quenched averages of the density of states and conductances

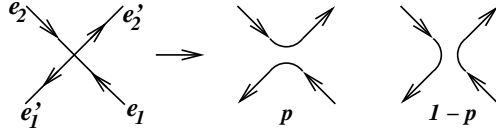


Figure 4: The two ways to decompose a node of  $\mathcal{G}$ . Note that in general this does not have to be planar, although for the L-lattice (Fig. 2) it is.

to observables of a classical random walk model on the same graph  $\mathcal{G}$ . We restrict attention to graphs with exactly 2 incoming and 2 outgoing edges. The general case is considered in Ref. [11] and is considerably more verbose.

Let us first define the corresponding classical problem. Starting with a given closed graph  $\mathcal{G}$ , to each node with incoming edges  $(e_1, e_2)$  and outgoing edges  $(e'_1, e'_2)$  associate its two possible *decompositions*  $((e'_1, e_1), (e'_2, e_2))$  and  $((e'_2, e_1), (e'_1, e_2))$ , corresponding to the two distinct ways of passing twice through the node without using a given edge more than once, irrespective of the order in which the edges are used. This is illustrated in Fig. 4. To each decomposition assign a probability  $p_n = \cos^2 \theta_n$  or  $1 - p_n = \sin^2 \theta_n$ , corresponding to the  $S$ -matrix in (2). Doing this for each node in  $\mathcal{G}$  gives a decomposition of  $\mathcal{G}$  into a union of closed loops. There are  $2^{|\mathcal{G}|}$  such decompositions, where  $|\mathcal{G}|$  is the total number of nodes, and the assigned probabilities give a product measure on the set of decompositions.

We now state the two main theorems. We use the symbol  $\overline{A}$  to denote a quenched average in the original quantum network model. Let  $P(L, e)$  be the probability that the edge  $e$  lies on a closed loop of length  $L$  in the classical problem.

**Theorem 1.**  $\overline{G(e_f, e_i, z)}$  vanishes unless  $e_f = e_i$ , when it is given by

$$\text{Tr } \overline{G(e, e, z)} = \begin{cases} 2 - \sum_{L>0} P(L, e) z^{2L} & : |z| < 1 \\ \sum_{L>0} P(L, e) z^{-2L} & : |z| > 1 \end{cases} .$$

If we apply this to the density of states in (5) we find simply

$$\rho(\epsilon) = (1/2\pi) \left( 1 - \sum_{L>0} P(L) \cos(2L\epsilon) \right), \quad (6)$$

where  $P(L) = (|\mathcal{G}|)^{-1} \sum_e P(L, e)$ , the probability that a edge chosen at random lies on a loop of length  $L$ . Note that if this distribution decays sufficiently fast for large  $L$ ,  $\rho(\epsilon)$  is expected to be analytic, while if it decays as a power law,  $\rho(\epsilon)$  will have a power law singularity at  $\epsilon = 0$ .

For an open graph with external contacts  $C_{\text{in}}$  and  $C_{\text{out}}$ , the decomposition of  $\mathcal{G}$  can also lead to open paths connecting edges in  $C_{\text{in}}$  to those in  $C_{\text{out}}$ . In this case, for the conductance, we have

**Theorem 2.** *The mean conductance is*

$$\overline{g} = 2 \sum_{e_{\text{in}} \in C_{\text{in}}} \sum_{e_{\text{out}} \in C_{\text{out}}} P(e_{\text{out}}, e_{\text{in}}),$$

where  $P(e_{\text{out}}, e_{\text{in}})$  is the probability that an open path from  $e_{\text{in}}$  to  $e_{\text{out}}$  exists. That is,  $\overline{g}$  is twice the mean number of open paths connecting  $C_{\text{in}}$  to  $C_{\text{out}}$ .

We describe the proof of these two Theorems using the supersymmetric path integral method of Ref. [11]: the combinatorial method in Ref. [10] is perhaps more illustrative of why the result holds, but it involves heavier algebra.

In the standard way, the Green function  $G$ , being the inverse of a matrix, may be written as a gaussian integral over commuting (bosonic) variables. The notation is a little cumbersome but the basic idea is simple. Label each end of a given edge  $e$  by  $e_R$  and  $e_L$ , in the direction of propagation  $e_R \rightarrow e_L$ . Introduce complex integration variables  $b_R(e)$  and  $b_L(e)$ , each of which is a 2-component column vector in the  $SU(2)$  space. Then

$$G(e_f, e_i; z) = \langle b_L(e_f) b_L(e_i)^\dagger \rangle = \frac{\int \prod_e [db_L(e)][db_R(e)] b_L(e_f) b_L(e_i)^\dagger e^{W[b]}}{\int \prod_e [db_L(e)][db_R(e)] e^{W[b]}} \quad (7)$$

where  $W[b] = W_{\text{edge}} + W_{\text{node}}$  and

$$W_{\text{edge}} = z \sum_e b_L^\dagger(e) U_e b_R(e), \quad W_{\text{node}} = \sum_n \sum_{ji} b_R^\dagger(e'_j) S_{ji} b_L(e_i).$$

We use the notation  $\langle \dots \rangle$  to denote averages with respect to this gaussian measure. The measure for each integration is

$$\int [db] = (1/\pi^2) \int e^{-b^\dagger b} d\text{Re } b d\text{Im } b.$$

For a finite graph there are a finite number of integrations and the integral is convergent for  $|z| < 1$ .

The next step is to average over the quenched random matrices  $U_e$ . As usual this is difficult because these appear in both the numerator and denominator of (7). This can be addressed using replicas, or, much more effectively in this case, by adding an anticommuting (fermionic) copy  $(f, \bar{f})$  of each pair bosonic variables  $(b, b^\dagger)$ . Note that each  $f$  is also a 2-component column vector in  $SU(2)$  space, and each  $\bar{f}$  a row vector. The Grassman integration over these is defined by

$$\int [df] = \int e^{-\bar{f} f} df d\bar{f},$$

where

$$\int [df] f = \int [df] \bar{f} = 0 \quad \text{and} \quad \int [df] 1 = \int [df] f \bar{f} = 1.$$

Integrating over these cancels the denominator in (7) so that

$$G(e_f, e_i; z) = \int \prod_e [db_L(e)][db_R(e)][df_L(e)][df_R(e)] f_L(e_f) \bar{f}_L(e_i) e^{W[b]+W[f]}. \quad (8)$$

The action  $W[b] + W[f]$  is supersymmetric under rotating bosons into fermions and *vice versa*, so we can replace the bosonic fields at  $e_i$  and  $e_f$  by fermionic ones and consider  $\langle f_L(e_f) \bar{f}_L(e_i) \rangle$ .

Now consider the average over  $U$  on a given edge. This has the form

$$\int dU \exp(z b_L^\dagger U b_R + z \bar{f}_L U f_R). \quad (9)$$

Because the anticommuting fields square to zero, the expansion of the exponential in powers of the second term terminates at second order. The gauge symmetry discussed earlier shows that the purely bosonic zeroth order term is in fact independent of  $b_L^\dagger$  and  $b_R$  and is in fact unity. The second order term is also straightforward: carefully using the anticommuting property we see that is actually proportional to  $\det U = 1$ , times the determinant of the  $SU(2)$  matrix of fermion bilinears with elements  $\bar{f}_{Li} f_{Rj}$ , where  $i$  and  $j$  take the values 1 or 2. The first order term then simply converts this into something supersymmetric. The conclusion is that the integral (9) equals  $1 + \frac{1}{2} z^2 \det \mathbf{M}$  where the  $2 \times 2$  matrix  $\mathbf{M}$  has components  $M_{ij} = b_{Li}^\dagger b_{Rj} + \bar{f}_{Li} f_{Rj}$ . This can be rearranged in the form

$$1 + z^2 [(1/\sqrt{2})(b_{L1}^\dagger \bar{f}_{L2} - b_{L2}^\dagger \bar{f}_{L1})] [(1/\sqrt{2})(b_{R1} f_{R2} - b_{R2} f_{R1})] + z^2 [\bar{f}_{L1} \bar{f}_{L2}] [f_{R2} f_{R1}].$$

Each expression in square brackets is an antisymmetric  $SU(2)$  singlet. The three terms above describe the propagation of either nothing, a fermion-boson ( $fb$ ) singlet, or a fermion-fermion ( $ff$ ) singlet along the edge  $e$ . This is a remarkable simplification: before the quenched average, each edge may be traversed many times, corresponding to the propagation of multi-particle states. It is this which gives one of the principle simplifications of the  $SU(2)$  case, that does not happen for  $U(1)$ , one of the reasons this is much more difficult.

This result shows that single fermions or bosons cannot propagate alone, so  $\overline{G(e_f, e_i)} = 0$  if  $e_f \neq e_i$ . A non-zero correlation function is however

$$\langle f_1(e_f) f_2(e_f) \bar{f}_2(e_i) \bar{f}_1(e_i) \rangle = \overline{G_{11} G_{12} - G_{21} G_{22}} = \overline{\det G(e_f, e_i, z)} \quad (10)$$

Now  $G$ , being a real linear combination of products of  $SU(2)$  matrices, can in fact always be written in the form  $\lambda \tilde{G}$  where  $\lambda$  is real and  $\tilde{G} \in SU(2)$ .<sup>2</sup> Hence  $\det G = \lambda^2$  and  $G^\dagger G = \lambda^2 \mathbf{1}$ , so  $\text{Tr } G^\dagger G = 2 \det G$ . When  $z = 1$  this gives the point conductance between  $e_i$  and  $e_f$ .

When  $e_i = e_f = e$ , however, we can always insert a pair of fermion fields  $f_2(e) \bar{f}_2(e)$  into the correlator  $\langle f_1(e) \bar{f}_1(e) \rangle$  at no cost, so that in fact

$$\overline{G(e, e; z)_{11}} = \overline{G(e, e; z)_{22}} = \overline{\det G(e, e; z)}.$$

Thus both the mean density of states and the mean conductance are proportional to  $\overline{\det G}$  and therefore are given by the correlation function (10).

The next step is to consider propagation through the nodes. Note that we can now drop the distinction between  $b_R$  and  $b_L$ , etc. The contribution from a given node takes the form

$$\prod_i A_{\alpha'_i}(e'_i) \mathcal{S} \prod_j A_{\alpha_j}^\dagger(e_j), \quad (11)$$

---

<sup>2</sup>This follows from the representation  $U = \cos \alpha + i(\sigma \cdot \mathbf{n}) \sin \alpha$ .

where  $A_1 = 1$ ,  $A_2 = (1/\sqrt{2})(b_1 f_2 - b_2 f_1)$ ,  $A_3 = f_1 f_2$ , and

$$\mathcal{S} = \exp \left( \sum_{ij} b_i^\dagger S_{ij} b_j + \bar{f}_i S_{ij} f_j \right),$$

where  $S_{ij}$  is the matrix in (2). Since this expression conserves fermion and boson number, it follows that the total numbers of  $(fb)$  and  $(ff)$  singlets are also conserved. Also, only terms second order in the  $S_{ij}$  survive. In fact, after a little algebra (11) reduces to<sup>3</sup>

$$\delta_{\alpha'_1 \alpha_1} \delta_{\alpha'_2 \alpha_2} S_{11} S_{22} - \delta_{\alpha'_2 \alpha_1} \delta_{\alpha'_1 \alpha_2} S_{21} S_{12} = \delta_{\alpha'_1 \alpha_1} \delta_{\alpha'_2 \alpha_2} \cos^2 \theta_n + \delta_{\alpha'_2 \alpha_1} \delta_{\alpha'_1 \alpha_2} \sin^2 \theta_n.$$

These two terms correspond to the decomposition of the node  $n$  described earlier. It shows that, on performing the quenched average, the quantum network model is equivalent to a classical one in which  $\mathcal{G}$  is decomposed into disjoint loops, and along each loop propagates either an  $(fb)$  singlet, an  $(ff)$  singlet, or nothing. Theorems (3,3) now follow straightforwardly. We argued above that the mean diagonal Green function  $\overline{G(e, e; z)}$  is given by the  $(ff)$  correlation function  $\langle [f_1(e) f_2(e)] [\bar{f}_1(e) \bar{f}_2(e)] \rangle$ . So, in each decomposition of  $\mathcal{G}$ , there must be an  $(ff)$  pair running around the unique loop containing  $e$ . This gets weighted by a factor  $z^{2L}$ . Around all the other loops we can have either an  $(ff)$  pair, a  $(bf)$  pair, or just 1. The  $(ff)$  pair, being itself bosonic, gives  $z^{2L}$  for a loop of length  $L$ , while the  $(bf)$  pair, being fermionic, gives  $-z^{2L}$ . These two cancel (by supersymmetry), leaving a factor 1 for every loop other than the one containing  $e$ . The argument for Theorem 3 for the conductance works in the same way.

Note that these methods may be extended to the quenched averages of other observables in the quantum model, although the density of states and the conductance are most important. However not all quantities of interest can be treated in this fashion. For example, the fluctuations in the conductance involve

$$\overline{(G(e_{\text{out}}, e_{\text{in}})^\dagger G(e_{\text{out}}, e_{\text{in}}))^2},$$

and, in order to treat this, we would need to double the number of degrees of freedom in the integral representation. Many of the formulas which are special to  $\text{SU}(2)$  integrations then no longer hold. In this context it is important to note that the conductance fluctuations in the quantum model are *not* given by the fluctuations in the number of paths connecting the two contacts in the classical model. (If this were the case, the quantum system would be behaving completely classically!)

An amusing application[10] of the general theorems is to consider single edge  $e$ , closed on itself, but take  $U_e \in \text{Sp}(N)$  with  $N$  even and  $> 2$  in general. A general  $\text{Sp}(N)$  matrix may be built up in terms of successive  $\text{Sp}(2)$  rotations in overlapping 2-dimensional subspaces. For example for  $\text{Sp}(4)$  we may write a general matrix in the form

$$\frac{1}{\sqrt{2}} \begin{pmatrix} U_1 & 0 \\ 0 & U_2 \end{pmatrix} \begin{pmatrix} \mathbf{1} & \mathbf{1} \\ -\mathbf{1} & \mathbf{1} \end{pmatrix} \quad (12)$$

---

<sup>3</sup>In Ref. [11] this was carried out for a general node of arbitrary coordination, with excruciating algebra.



Figure 5: Graph corresponding to a single link in the  $\text{Sp}(4)$  model, and its topologically distinct decompositions. Each node corresponds to the  $S$ -matrix which is the second factor in (12), so each term in the decomposition is equally weighted.

where  $U_1$  and  $U_2$  are independent  $\text{Sp}(2)$  matrices. If these are drawn from the invariant measure on  $\text{Sp}(2)$ , then the product of a large number of independent such matrices will converge to the invariant measure on  $\text{Sp}(4)$ . Thus, in a particular  $\text{Sp}(2)$  basis,  $\mathcal{G}$  has the form shown in Fig. 5. After applying Theorem 3, each decomposition corresponds to a permutation of the different channels corresponding to the basis chosen in (12). This generalizes to arbitrary  $N$ . If we now connect opposite ends of Fig. 5 to make a closed graph, we find, after the decomposition, all possible lengths  $L$  of loops from 1 to  $\frac{1}{2}N$ , with equal probabilities. Thus  $P(L) = 2/N$  for  $1 \leq L \leq \frac{1}{2}N$ , and zero otherwise. Using (6), this gives for the density of eigenvalues of a random  $\text{Sp}(N)$  matrix

$$\rho(\epsilon) = \frac{N+1}{2\pi N} \left( 1 - \frac{\sin(N+1)\epsilon}{(N+1)\sin\epsilon} \right),$$

in agreement with Ref. [12].

## 4 Two-dimensional models

In this section we discuss the consequences of the main theorems for specific 2d lattices relevant to physical problems.

### 4.1 The L-lattice

This is the lattice, illustrated in Fig. 2, used by the original Chalker-Coddington model for the quantum Hall plateau transition. The reasons for choosing this lattice were discussed in Sec. 1. In the class C version of this, the same lattice is used, the only difference being that the quenched random  $U(1)$  phases on each edge are replaced with  $SU(2)$  matrices. We also recall that, because of the checkerboard nature of the potential, where even plaquettes correspond to  $V > 0$  and odd ones to  $V < 0$ , the angles  $\theta_n$ , which represent the degree of anisotropy of the tunnelling at the nodes, are in fact staggered:  $\theta_n = \theta$  on the even sublattice, and  $(\pi/2) - \theta$  on the odd sublattice. Thus for  $\theta = 0$  all the loops in the decomposition of  $\mathcal{G}$  will be the minimum size allowed, surrounding the even plaquettes, and for  $\theta = \pi/2$  they will surround the odd plaquettes. Away from these extreme values, the loops will be larger. If there is a single transition it must occur at  $\theta = \pi/4$ .

The mapping to square lattice bond percolation for this model is exact. Consider independent bond percolation on the square lattice  $\mathcal{L}'$ , rotated by  $45^\circ$  with respect to the original, whose sites lie at the centers of the even plaquettes of the original lattice. See

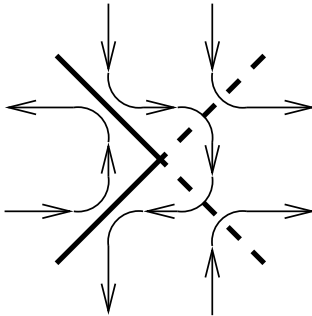


Figure 6: The mapping between decompositions of the L-lattice and bond percolation on the lattice  $\mathcal{L}'$ . Open bonds are shown as thick lines, closed as dashed lines.

Fig. 6. Each edge of  $\mathcal{L}'$  intersects a node of the original one. We declare it to be open, with probability  $p = \cos^2 \theta$ , or closed, with probability  $1 - p = \sin^2 \theta$ , according to the way the node is decomposed in the classical loop model on  $\mathcal{G}$ . There is thus a 1-1 correspondence between decompositions of  $\mathcal{G}$  and bond percolation configurations on  $\mathcal{L}'$ . We can also consider the dual lattice  $\mathcal{L}''$  whose vertices are at the centers of the odd plaquettes of the original lattice. Each edge of this lattice crosses a unique edge of  $\mathcal{L}'$ , and we declare it to be open, with probability  $1 - p$ , if the corresponding edge of  $\mathcal{L}'$  is closed, and *vice versa*. For each percolation configuration on  $\mathcal{L}'$ , there is a corresponding dual configuration on  $\mathcal{L}''$ . The clusters and dual clusters fill the plane without intersecting each other. (For this purpose it is necessary to regard single isolated sites as clusters.) Close to  $p_c = \frac{1}{2}$  many clusters nest inside dual clusters and *vice versa*.

For a given decomposition of  $\mathcal{G}$ , the loops give the *hulls* of percolation clusters on  $\mathcal{L}'$  and dual clusters on  $\mathcal{L}''$ . For a closed simply connected lattice  $\mathcal{G}$ , these are closed curves which simultaneously circumscribe a cluster and inscribe a dual cluster, or *vice versa*. For open boundary conditions, some of these curves may begin and end on the boundary.

From this mapping to 2d percolation, and known exact and conjectured results about the latter, many results about the SU(2) network model on the L-lattice may be deduced[8]. At the transition, the conductance between two bulk points a distance  $r$  apart is given by the probability that they are on the same loop, which is known to decay as  $|r|^{-2x_1}$  where  $x_1 = \frac{1}{4}$  [13]. The conductance of a rectangular sample with contacts along opposite edges is given by the mean number of hulls which cross the sample. At the critical point this depends only its aspect ratio  $L_1/L_2$ , in a complicated but calculable way[14]. For  $L_1/L_2 \gg 1$  (where  $L_1$  is the length of the contacts) it goes like  $\bar{g}(L_1/L_2)$  where  $\bar{g}$  is the universal critical conductance which, from conformal field theory results applied to percolation, takes the value  $\sqrt{3}/2$ . [14] In Sec. 3 we showed that the mean density of states is given by the probability  $P(L)$  that a given edge is on a loop of length  $L$ . At criticality, this probability scales like  $L^{-x_1}$  where  $d_f = 2 - x_1 = \frac{7}{4}$  is the fractal dimension of percolation hulls.[13]. Also  $|z - 1| \propto |E|$ , which is conjugate to  $L$ , has RG eigenvalue  $y_1 = 2 - x_1$ . This means that the singular part of the mean density of states behaves

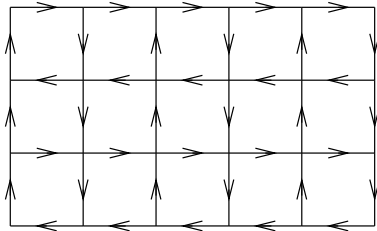


Figure 7: The Manhattan lattice.

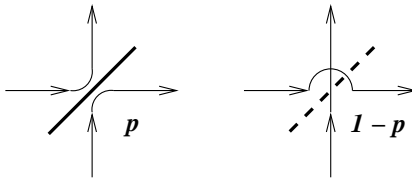


Figure 8: The decomposition of each node of the Manhattan lattice and its relation to percolation on  $\mathcal{L}'$ . Open bonds shown as solid thick lines, closed as dashed.

like[8]

$$\overline{\rho(E)} \sim |E|^{x_1/y_1} = |E|^{1/7}.$$

A number of other exponents, including the usual percolation correlation length exponent  $\nu = \frac{4}{3}$ , were identified in the physics of the spin quantum Hall transition in Ref. [8].

## 4.2 The Manhattan lattice

Although the  $L$ -lattice is the natural candidate for studying the spin quantum Hall transition, the mapping discussed in Sec. 3 is of course valid for any orientation of the edges of a square lattice, and one can legitimately ask whether other possibilities lead to interesting physics. The expectation, based on the continuum classification of localization universality classes, is that unless there is some special symmetry, such as occurs for the  $L$ -lattice with its sublattice symmetry, all states in 2d will be exponentially localized and therefore almost all loops in the classical model will have finite length. This was studied for the Manhattan lattice in Ref. [15]. On this lattice all edges in the same row or column are oriented in the same direction, and these alternate, see Fig. 7. This resembles the one-way system of streets and avenues in Manhattan. At each corner, the driver can go straight on, or turn either left or right according to the parity of the intersection.

Consider an  $SU(2)$  network model on this lattice. The decomposition of the lattice corresponds to replacing each node either by a crossing, with probability  $1 - p$ , say, or an avoidance, with probability  $p$  (see Fig. 8). Note that in this case the loops on the decomposed lattice are in general non-planar. Nevertheless it is possible to make rigorous progress using a mapping to percolation, owing to the sublattice structure. Consider once again bond percolation on the  $45^\circ$ -rotated lattice  $\mathcal{L}'$  (see Fig. 8). An edge is declared open if the corresponding node is decomposed in such a way that the paths turn by  $90^\circ$ ,

as shown. The open edges once again form connected clusters which enclose, and are enclosed by, percolation hulls, and similarly for the dual clusters. A little reflection shows that each loop of the decomposed Manhattan lattice is constrained to lie on or between neighboring hulls which enclose a dual cluster. For  $p > p_c = \frac{1}{2}$  the dual clusters are almost surely finite, and therefore so are their surrounding hulls, and therefore also the loops of the decomposed  $\mathcal{G}$ . Therefore for  $p > \frac{1}{2}$  the SU(2) network model on the Manhattan lattice is in the localized phase. An unproven conjecture, consistent with our expectations for Anderson localization in 2d, is that this happens for all  $p > 0$ . Simulations[15] of the classical loop model indicate that this is the case for  $p > 0.2$ . The field theory arguments to be discussed later indicate that there should always be a finite localization length, diverging as  $\xi \sim \exp(\text{const.}/p^3)$  as  $p \rightarrow 0$ .

### 4.3 Other 2d lattices

We may consider other orientations of the square lattice. In general a given orientation corresponds to a configuration of the six-vertex model, which satisfies the ‘ice rule’ that there are two incoming and two outgoing arrows at each vertex, or node. The number of such allowed configurations grows exponentially with the size of the lattice, but we could, for example, consider a randomly oriented lattice in which the weights for different types of node are given by the 6-vertex model. In that case the L-lattice and Manhattan lattice are just particular extreme points of the parameter space. Once again we can associate an edge of the lattice  $\mathcal{L}'$  or  $\mathcal{L}''$  with the decomposition of a node where the path has to turn. These edges can be thought of as two-sided mirrors, reflecting all the paths which impinge on either side. The study of these ‘mirror models’ as models for classical localization has been extensive (see, for example Ref. [16], and references quoted therein), although on the whole only simulational results are available. However it is important to realize that arbitrary mirror models do not in general lead to a unique orientation for the edges: a path may traverse a given edge in both directions. Thus the set of mirror configurations corresponding to quantum network models is a subset, and it would be wrong to infer general conclusions about these from the study of the wider problem. Nevertheless, one expects that, for a sufficiently high density of randomly oriented mirrors, the paths are finite and so the states are localized. An interesting and unresolved question, however, is what happens at low mirror density, when the mean free path is large. Expectations from quantum localization would then suggest that the paths in such models are still localized on large enough scales, unless there is some special symmetry like that of the L-lattice.

## 5 Three-dimensional models

We now discuss some results for class C network models on 3d lattices. It is possible, of course, to consider layered 2d lattices which might be used as models for quantum Hall physics in multilayered systems. For example, in a bilayer system consisting of two coupled L-lattices, depending on the strength of the coupling between the layers, one

expects to see either two separate transitions between states of Hall conductance 0, 1 and 2. These can be simply understood in terms of the classical model and an equivalent percolation problem.[17] However, such models do not capture some of the important properties of real bilayer systems which depend on electron-electron interactions.

One motivation for studying truly 3d class C network models is to shed light on the physics of the localization transition in 3d. So far, these have been carried out either numerically or by mapping to 3d percolation. However the restriction to four-fold coordination in order that the equivalent classical model has non-negative weights[11] means that it is necessary to use loose-packed lattices.

## 5.1 Diamond lattice

The most extensive numerical simulations have been carried out on the diamond lattice.[18] Although this lattice has cubic symmetry, assigning the orientations of the edges breaks this down to tetragonal, inducing an anisotropy. However, numerical tests show that this is not very great, giving, for example, a ratio of about 1.1 between the conductances in the two distinct directions in the conducting phase. As expected, the model exhibits a sharp transition at  $p = p_c$  between an insulating phase and a conducting phase. This is shown, for example, in data for the conductance  $G(p, L)$  of a cubic sample of linear size  $L$ , which, according to the Theorem 3, is given by the mean number of open paths between two opposite faces. In the insulating phase  $p < p_c$  this should approach zero as  $L \rightarrow \infty$ , while for  $p > p_c$  we expect ohmic behavior with  $G(p, L) \sim \sigma(p)L$ . Close the critical points we expect finite-size scaling of the form

$$G(p, L) = f(L/\xi(p)),$$

where the localization length  $\xi(p) \sim |p - p_c|^{-\nu}$ . Thus the data should show collapse when plotted as a function of  $(p - p_c)L^{1/\nu}$ , and this is clearly exhibited in Fig. 9. The best fitted value for  $\nu$ , taking into account corrections to scaling, is[18]  $\nu = 0.9985 \pm 0.0015$ . The closeness of this value to unity, the value predicted by a first-order result  $\nu^{-1} = \epsilon + O(\epsilon^2)$  of the  $2 + \epsilon$ -expansion (see Sec. ?? and Ref. [24]) is remarkable, but perhaps a coincidence.

At  $p = p_c$ , the weighted number of return paths of length  $L$ , behaves as  $P(L) \sim L^{-x_1/y_1}$ , as discussed in Sec. 4.1. In Ref. [18] this exponent is denoted by  $2 - \tau$ , where numerically  $\tau = 2.184 \pm 0.003$ . This exponent is related to the fractal dimension  $d_f = y_1 = 3 - x_1$  of the paths at  $p_c$ , giving  $d_f = 2.534 \pm 0.009$ . By the same arguments as in Sec. 4.1, this gives, for example, the singular part of the density of states  $\rho(E) \sim |E|^{\tau-2}$ . Note that, because of the mapping to the classical problem for which far larger systems can be studied, the error bars on these exponents are much smaller than those quoted for the conventional 3d Anderson transition.

## 5.2 3d L-lattice and Manhattan lattice

It is possible to construct 3d oriented lattices with cubic symmetry which are direct analogues of the 2d L-lattice and Manhattan lattices discussed in Sec. 4 and for which

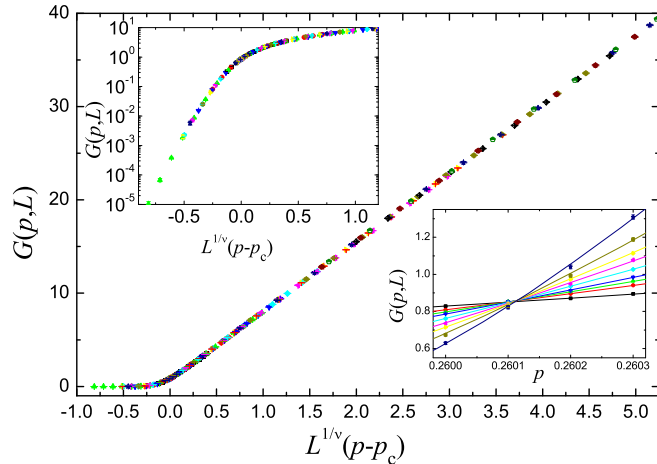


Figure 9: Conductance as a function of  $(p - p_c)L^{1/\nu}$ , illustrating scaling collapse. Upper inset: same data on a logarithmic scale. Lower inset: conductance as a function of  $p$  for several values of  $L$ . Lines are a scaling fit described in detail in Ref. [18]. (Reproduced from Ref. [18] with permission of the authors.)

the arguments relating the classical models to percolation can be generalized.

Consider two interpenetrating cubic lattices  $\mathcal{C}_1 \equiv \mathbf{Z}^3$  and  $\mathcal{C}_2 \equiv (\mathbf{Z} + \frac{1}{2})^3$ . Each face of  $\mathcal{C}_1$  intersects an edge of  $\mathcal{C}_2$  at its midpoint. The four faces of  $\mathcal{C}_2$  which meet along this edge intersect the given face of  $\mathcal{C}_1$  along two mutually perpendicular lines, also perpendicular to the edge (see Fig. 10). These lines form part of the lattice  $\mathcal{G}$ . The same is true, interchanging the roles of  $\mathcal{C}_1$  and  $\mathcal{C}_2$ . The full graph  $\mathcal{G}$  is the lattice formed by the intersection of the faces of  $\mathcal{C}_1$  with those of  $\mathcal{C}_2$ . The nodes of  $\mathcal{G}$  lie on the midpoints of the edges of  $\mathcal{C}_1$  (the centers of the faces of  $\mathcal{C}_2$ ) and *vice versa*, and have coordination number 4. Clearly  $\mathcal{G}$  has cubic symmetry.

For the L-lattice on  $\mathcal{G}$ , the orientation of the edges is chosen so that each node looks like the nodes of the 2d L-lattice, as in Fig. 10. There is an overall 2-fold degeneracy in assigning these, but once the orientation at one node is fixed, so are the rest. The  $S$ -matrices of the network model, and the corresponding probabilities  $p$  and  $1 - p$  for the decomposition of  $\mathcal{G}$  are assigned consistent with the percolation mapping now to be described.

The sites of  $\mathcal{C}_1$  may be assigned to even and odd sublattices  $\mathcal{C}'_1$  and  $\mathcal{C}''_1$  according to whether the sum of the coordinates is even or odd. Each of these lattices is in fact a face-centered cubic (fcc) lattice. Now consider nearest neighbor bond percolation on  $\mathcal{C}'_1$ . Each nearest neighbor edge of  $\mathcal{C}'_1$  intersects the midpoint of an edge of  $\mathcal{C}_2$ , along which 4 faces of  $\mathcal{C}_2$  intersect. A decomposition of this edge consists in connecting up these faces in neighboring pairs, as in Fig. 11.

For each edge there are two possible decompositions, and we can do this in such a way

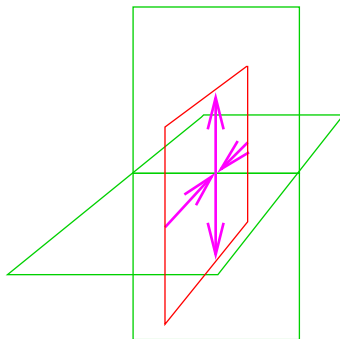


Figure 10: A node of  $\mathcal{G}$  (purple) is formed by the intersection of four faces of  $\mathcal{C}_2$  (green) and one face of  $\mathcal{C}_1$  (red), and *vice versa*. The orientation shown corresponds to the 3d L-lattice.

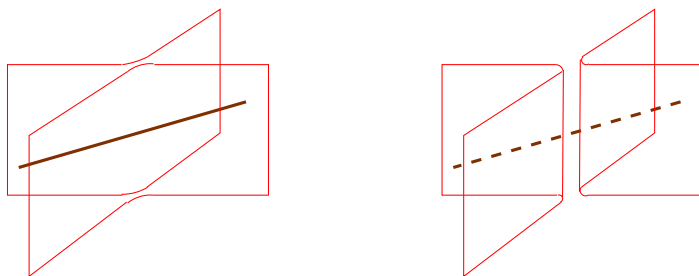


Figure 11: Decomposition of the four faces (in red) at an edge of  $\mathcal{C}_1$  corresponding to bond percolation (bonds shown in brown) on an fcc sublattice of  $\mathcal{C}_2$ .

that if the corresponding edge of the percolation problem on  $\mathcal{C}'_1$  is open, it passes between the connecting pairs (see Fig. 11), just as in Fig. 6 in 2d. If on the other hand the edge is closed, then it intersects both pairs. Equivalently, we can consider percolation on the ‘dual’ fcc lattice  $\mathcal{C}''_1$ . Each edge of this lattice intersects one edge of  $\mathcal{C}'_1$  at the midpoint of an edge of  $\mathcal{C}_2$ . We declare the edge of  $\mathcal{C}''_1$  to be open if the intersecting edge of  $\mathcal{C}'_1$  is closed, and *vice versa*.

For a finite lattice, each decomposition of the edges of  $\mathcal{C}_2$  divides the faces of  $\mathcal{C}_2$  into a union of dense, non-intersecting, closed surfaces, in the same way that a decomposition of the corresponding nodes of the 2d square lattice divides the edges into non-intersecting closed loops. These closed surfaces form the hulls of the bond percolation clusters on the fcc lattice  $\mathcal{C}'_1$  and its dual  $\mathcal{C}''_1$ . That is, each closed surface either touches a unique cluster externally and a unique dual cluster internally, or *vice versa*.

However, this is only half the description. The edges of  $\mathcal{G}$  are formed by the intersection of the faces of  $\mathcal{C}_1$  with those of  $\mathcal{C}_2$ . Therefore we need to also decompose the faces of  $\mathcal{C}_1$ . This is carried consistent with another, independent, percolation problem on an fcc sublattice  $\mathcal{C}'_2$  of  $\mathcal{C}_2$ , and its dual  $\mathcal{C}''_2$ . To each double decomposition of the faces of  $\mathcal{C}_1$  into closed non-intersecting surfaces, and similarly of the faces of  $\mathcal{C}_2$ , corresponds a unique decomposition of  $\mathcal{G}$  into closed loops.

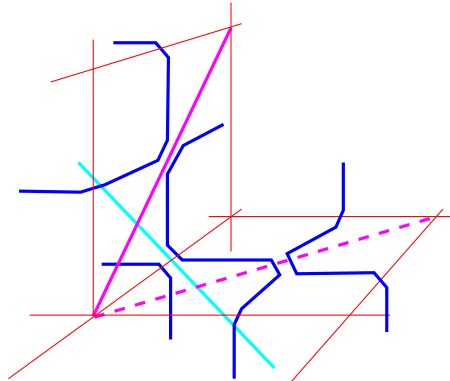


Figure 12: A decomposition of  $\mathcal{G}$  on the 3d L-lattice, showing how the loops (blue) reflect off the open bonds of percolation on the fcc lattices  $\mathcal{C}'_1$  (solid magenta lines) and  $\mathcal{C}'_2$  (solid turquoise lines).

This is the classical loop model which we seek. Unlike the 2d case, it corresponds to *two* independent percolation problems, one on an fcc lattice of  $\mathcal{C}_1$ , the other on an fcc sublattice of  $\mathcal{C}_2$ . Each closed loop of  $\mathcal{G}$  is formed by the intersection of a closed surface made up of faces of  $\mathcal{C}_1$  and a closed surface made up of faces of  $\mathcal{C}_2$ . (It is of course possible that such pairs of closed surfaces intersect in more than one loop of  $\mathcal{G}$ , or not at all.) It alternately ‘reflects’ off an open edge of percolation on  $\mathcal{C}'_1$  (or an open dual edge of  $\mathcal{C}''_1$ ), then an open edge of  $\mathcal{C}'_2$  or of  $\mathcal{C}''_2$ , and so on (see Fig. 12).

We now discuss the physics of this model and its implications for the class C network model. In principle we can assign different probabilities,  $p_1$  and  $p_2$ , to the two independent percolation problems on  $\mathcal{C}_1$  and  $\mathcal{C}_2$ . The phase diagram is symmetric under the duality symmetry  $p_j \rightarrow 1 - p_j$ , so we can restrict attention to the quadrant  $p_1 \leq \frac{1}{2}$ ,  $p_2 \leq \frac{1}{2}$ . For either  $p_1$  or  $p_2$  less than the bond percolation threshold  $p_c^{\text{fcc}} \approx 0.12$  [19], since the clusters are finite so are the hulls on either  $\mathcal{C}_1$  or  $\mathcal{C}_2$  (or both), and, since the loops on  $\mathcal{G}$  are formed by their intersection, these must be finite also, corresponding to a localized phase. Preliminary simulations of the model[20] for values of  $p_j$  close to  $\frac{1}{2}$  appear to show that the loops are no longer finite, but, unlike the case of the diamond lattice[18], neither are they simple random walks on large scales with fractal dimension 2, as would be expected of a sample exhibiting ohmic behavior. In fact, their fractal dimension appears to be close to 3, indicating that they are space filling. This may be a pathology of this model. It is known that the fractal dimension of cluster boundaries for  $p > p_c$  is 3 – that is, a finite fraction of the infinite cluster, which has dimension 3 because it contains a finite fraction of the sites, is on its boundary. The loops for  $p > p_c$  are formed by the intersection of random such  $d_f = 3$  objects, so it is perhaps not surprising that they should also have  $d_f = 3$ .

For this reason it may be more useful to consider a 3d version of the Manhattan lattice. This is based on the same graph  $\mathcal{G}$ , but the edges are oriented so that along each line through the lattice they point in the same direction, and the lines alternate direction transversally. As in the 2d case, the probability of turning at a given node is  $p$  and of

going straight on  $1 - p$ . (In principle we could again take different values of  $p$  at the two types of nodes corresponding to  $\mathcal{C}_1$  and  $\mathcal{C}_2$ .) Analogously with the 2d case (see Sec. 4.2), we can introduce an associated percolation problem on fcc sublattices of  $\mathcal{C}_2$  and  $\mathcal{C}_1$ , so that if, in the decomposition of  $\mathcal{G}$ , the paths turn at a given node, they reflect off an open edge. This means that, as in 2d, they are constrained to lie on regions occupied by the dual clusters of each percolation problem. Thus, for  $p > 1 - p_c^{\text{fcc}} \approx 0.88$ , the loops of  $\mathcal{G}$  are almost surely finite in length, corresponding to the existence of a localized phase of the corresponding class C network model.

On the other hand, for small  $p$  we expect a finite fraction of the paths to escape to infinity on a infinite lattice, corresponding to extended states. In this case the particle following a path will, almost, all the time, go straight ahead, with only a small probability  $p \ll 1$  of turning. In this case, the whether the particle has traversed an even or odd number of edges should be unimportant, leading to an effective simple random walk with diffusion constant  $O(p^{-1})$  on intermediate distance scales. On larger scales, the walk may revisit regions it has in the past, but, unlike the case of 2d, this is unlikely because the 3d random walk is not recurrent. However, as appealing as this argument may be, it is not rigorous, and indeed its proof appears to be of the same order of difficulty as showing that the ‘true’ self-avoiding walk in 3d is asymptotically gaussian[21, 22]. Thus, at this stage, a proof of the existence of extended states in this class of network models remains elusive.

## 6 Summary and further remarks

We have shown how the quantum  $\rightarrow$  classical mapping for class C network models helps to gain insight into the nature of Anderson localization in both two and three dimensions. These models have direct physical relevance in systems where time-reversal symmetry is broken but spin rotational symmetry is preserved. The classical models correspond to deterministic motion in a random medium with two-sided mirrors, or, equivalently, certain kinds of history-dependent random walks. On some lattices, including the important examples of the L and Manhattan lattices, the paths are associated with the hulls of percolation clusters, and rigorous information can be inferred on whether the corresponding quantum model is in a localized or extended phase.

However, there are a number of unresolved questions. Although the diamond lattice and 3d Manhattan lattice discussed in Sec. 5 are expected to exhibit an Anderson transition, there is as yet no proof of the existence of an extended phase in which the motion is asymptotically diffusive, although this is strongly indicated on both numerical and other grounds. The relation of these models to other types of history-dependent random walks, such as the ‘true’ self-avoiding walk, in which the walk avoids regions it has visited in the past, is also unclear. Like Anderson localization,  $d = 2$  is a critical dimension for the true self-avoiding walk. However in this case the RG flows[22, 23] are to free random walks for  $d \geq 2$ , and to a non-trivial stable fixed point for  $d < 2$ , while for Anderson localization we expect to find a non-trivial unstable fixed point for  $d > 2$ . This suggests that the

two problems are related by a change of sign of the interaction. However the analysis of Peliti and Obukhov[23] shows that for history-dependent random walks there are in fact three coupling constants which are potentially important near  $d = 2$ . An attempt to fit the walks on the 2d Manhattan lattice into this picture was made in Ref. [15]. However this was not systematic and further work needs to be done in this direction. It should be noted, however, that a sigma-model analysis of the original class C quantum model does give the expected unstable fixed point for  $d > 2$ . [24]. A related question is that of the *upper* critical dimension for the transition in this model. The relation to interacting random walks suggests that this might be  $d = 4$ , as for ordinary polymers, but in this case the interactions are not simply repulsive, so this conclusion may not hold.

## Acknowledgements

I am especially grateful to John Chalker for many informative discussions of this subject over the years, as well as Ilya Gruzberg, Yacine Ikhlef, Andreas Ludwig, Adam Nahum, Aleks Owczarek, Nick Read, Tom Spencer, Bob Ziff and Martin Zirnbauer. This work was supported in part by EPSRC Grant EP/D050952/1.

## References

- [1] J. T. Chalker and P. D. Coddington, Percolation, tunnelling and the integer quantum Hall effect, *J. Phys. C*. **21**, 2665-2679, (1988).
- [2] R. E. Prange and R. Joynt, Conduction in a strong field in two dimensions: The quantum Hall effect, *Phys. Rev. B*. **25**, 2943-2946, (1982).
- [3] S. A. Trugman, Localization, percolation, and the quantum Hall effect, *Phys. Rev. B*. **27**, 7539-7546, (1983).
- [4] A. M. M. Pruisken, On localization in the theory of the quantized hall effect: A two-dimensional realization of the  $\theta$ -vacuum, *Nucl. Phys. B*. **235**, 277-298, (1984); I. Affleck, Critical behaviour of  $SU(n)$  quantum chains and topological non-linear  $\sigma$ -models, *Nucl. Phys. B*. **305**, 582-596, (1988); A. W. W. Ludwig, M. P. A. Fisher, R. Shankar, and G. Grinstein, Integer quantum Hall transition: An alternative approach and exact results, *Phys. Rev. B*. **50**, 7526-7552, (1994); M. R. Zirnbauer, Conformal field theory of the integer quantum Hall plateau transition, arXiv:hep-th/9905054 (unpublished).
- [5] T. Senthil, J. B. Marston and M. P. A. Fisher, Spin quantum Hall effect in unconventional superconductors, *Phys. Rev. B*. **60**, 4245-4254, (1999).
- [6] A. Altland and M. R. Zirnbauer, Nonstandard symmetry classes in mesoscopic normal-superconducting hybrid structures *Phys. Rev. B*. **55**, 1142-1161, (1997); M. R. Zirnbauer, Riemannian symmetric superspaces and their origin in random-matrix theory, *J. Math. Phys.*. **37**, 4986-5018, (1996).

- [7] V. Kagalovsky, B. Horovitz, Y. Avishai, Landau-level mixing and spin degeneracy in the quantum Hall effect, *Phys. Rev. B.* **55**, 7761-7770, (1997); V. Kagalovsky, B. Horovitz, Y. Avishai and J. T. Chalker, Quantum Hall Plateau Transitions in Disordered Superconductors, *Phys. Rev. Lett.* **82**, 3516-3519, (1999).
- [8] I. A. Gruzberg, A. W. W. Ludwig and N. Read, Exact Exponents for the Spin Quantum Hall Transition, *Phys. Rev. Lett.* **82**, 4524-4527, (1999).
- [9] S. Smirnov and W. Werner, Critical exponents for two-dimensional percolation, *Math. Res. Lett.* **8**, 729-744, (2001).
- [10] E. J. Beamond, J. Cardy and J. T. Chalker, Quantum and Classical Localisation, the spin Quantum Hall effect and generalisations, *Phys. Rev. B.* **65**, 214301-214310, (2002).
- [11] J. Cardy, Network Models in Class C on Arbitrary Graphs, *Comm. Math. Phys.* **258**, 87, (2003).
- [12] M. R. Zirnbauer, Supersymmetry for systems with unitary disorder: circular ensembles, *J. Phys. A.* **29**, 7113-7136, (1996).
- [13] B. Nienhuis, Critical behavior of two-dimensional spin models and charge asymmetry in the Coulomb gas, *J. Stat. Phys.* **34**, 731-761, (1984).
- [14] J. Cardy, Linking numbers for self-avoiding loops and percolation: application to the spin quantum Hall transition, *Phys. Rev. Lett.* **84**, 3507-3510, (2000).
- [15] E. J. Beamond, J. Cardy and A. L. Owczarek, Quantum and Classical Localisation and the Manhattan Lattice, *J. Phys. A.* **36**, 10251, (2003).
- [16] M. S. Cao and E. G. D. Cohen, Scaling of particle trajectories on a lattice, *J. Stat. Phys.* **87**, 147-178, (1997).
- [17] E. A. Beamond, Ph.D. thesis (unpublished).
- [18] M. Ortuño, A. M. Somoza and J. T. Chalker, Random Walks and Anderson Localization in a Three-Dimensional Class C Network Model, *Phys. Rev. Lett.* **102**, 070603-070606, (2009).
- [19] C. D. Lorenz and R. M. Ziff, Precise determination of the bond percolation thresholds and finite-size scaling corrections for the sc, fcc, and bcc lattices, *Phys. Rev. E.* **57**, 230236, (1998).
- [20] Y. Ikhlef, private communication.
- [21] R. T. Durrett and L. C. Rogers, Asymptotic Behaviour of Brownian Polymers, *Probab. Theory Related Fields* **92**, 337-349, (1992.)

- [22] D. J. Amit, G. Parisi and L. Peliti, The Asymptotic Behaviour of the ‘True’ Self-Avoiding Walk, *Phys. Rev. B.* **27**, 16351645, (1983).
- [23] S. P. Obukhov and L. Peliti, Renormalisation of the ‘true’ self-avoiding walk, *J. Phys. A.* **16**, L147-L151, (1983.)
- [24] T. Senthil, M. P. A. Fisher, L. Balents and C. Nayak, Quasiparticle Transport and Localization in High- $T_c$  Superconductors, *Phys. Rev. Lett.* **81**, 47044707, (1998); T. Senthil and M. P. A. Fisher, Quasiparticle density of states in dirty high- $T_c$  superconductors, *Phys. Rev. B.* **60**, 68936900, (1999).